Eur. Phys. J. D **29**, 397–408 (2004)
DOI: 10.1140/epjd/e2004-00048-8

THE EUROPEAN PHYSICAL JOURNAL D

Microfield fluctuations and radiative transitions in laser-generated strongly coupled plasmas

J. Marten and C. Toepffer[a]

Institut für Theoretische Physik II, Universität Erlangen, Staudtstr. 7, 91058 Erlangen, Germany

Received 7 January 2004
Published online 15 April 2004 –

Abstract. Previously unaccessible plasma states of matter can be produced by irradiation with powerful lasers. The interactions within the plasma shift and distort the spectral lines corresponding to radiative transitions. The shape of the spectra is determined by two frequencies characterizing the fluctuations of the electric microfield in the plasma and the Stark splitting of the lines. Traditionally the fluctuations due to the motion of the ions are considered as sufficiently slow and weak to be treated in a linear quasi-static approximation, while the electrons are accounted for in an instantaneous impact approximation. Here also the intermediate regimes and strongly correlated ions are investigated. For that purpose the microfield fluctuations are calculated by molecular dynamics computer simulations. They are then used as input in a numerical solution of the time-dependent Schrödinger equation for the radiating electron. The shape of the Ly_α–line in H and in Al is investigated in the intermediate regime. The calculations are in agreement with recent experiments on the Ly_α and Ly_γ lines in Al.

PACS. 32.30.Rj X-ray spectra – 32.70.Jz Line shapes, widths, and shifts – 52.25.Os Emission, absorption, and scattering of electromagnetic radiation – 52.65.Yy Molecular dynamics methods

1 Introduction

Due to the rapid progress of technology [1] previously unaccessible states of matter can be investigated by irradiation with powerful lasers. A few typical examples are: The compression of deuterium pellets for inertial fusion [2,3] and shock wave experiments to investigate possible phase transitions like the metalization of hydrogen [4], which are not only of large fundamental interest [5] but also important for astrophysical problems like the structure of the giant planets [6]. Such experiments require typically large lasers delivering pulses with PW power for $10^{-12\cdots-9}$ s. On the other hand femtosecond–table–top lasers deliver intensities beyond 10^{18} W/cm^2 on targets where the self-amplification of the electromagnetic fields by charge separation has been successfully exploited for the generation of particle jets [7]. The extreme plasma states created in the target after the laser irradiation can be analyzed spectroscopically [8] and the dynamics can be monitored in a time-resolved manner [9].

In comparison to isolated atoms or ions the interactions within a plasma shift and distort the spectral lines corresponding to radiative transitions. Spectroscopy is therefore a tool to diagnose the state of a plasma. Of particular importance are the fluctuations of the electric microfield $\vec{E}(t)$. For the shape of the spectral lines two frequencies are important: a field frequency $\omega_0 = |\dot{E}(t)/E|$ characterizing the fluctuations of the perturbing field and the splitting of spectral lines $\Delta\omega$ due to the Stark effect. The calculation of line shapes is facilitated by approximations which are valid in complementary extreme regimes [10]. If the shortest time scale is set by ω_0, the radiator is perturbed by a set of instantaneous collisions which need not be further resolved in time. This impact approximation is often valid to describe the perturbations due to swiftly moving plasma electrons. However, if the shortest time scale is set by $\Delta\omega$, it is only the probability distribution $P(E)$ of the electric field which matters. This quasi-static approximation is usually employed to account for the influence of the heavier, slowly moving plasma ions. Moreover, if the electric microfields are sufficiently weak, both $P(E)$ and the Stark splitting $\Delta\omega$ can be calculated perturbatively.

In the intermediate regime approximations have been proposed which generally involve severe assumptions and idealizations, they should therefore be regarded as model calculations. The hopes for a truly unified and practical theory were considered as dim [10]. Nevertheless progress has been made by treating the effect of the ions on the radiator in an effective independent-particle model (APEX) [11–13] as well as the Coulomb interaction between the electrons and the radiator beyond the

[a] e-mail: toepffer@theorie2.physik.uni-erlangen.de

dipole term [14]. These methods were applied to highly charged Ar ions in D plasmas [14–16]. In the present paper we want to study even stronger coupled systems, e.g. highly charged radiators in plasmas with highly charged ions. For that purpose we perform numerical simulations which cover a wide range of plasma densities and temperatures accessible in present experiments or in the near future. The simulations span the entire range between the impact and the quasi-static approximations. We explicitly solve the time-dependent Schrödinger equation for the radiator in the fluctuating microfield due to the other plasma particles. As we want to account for strong correlations in the plasma, the field fluctuations are obtained from molecular dynamics (MD) simulations.

The paper is organized as follows: in Section 2 we describe the radiating ion and its coupling to the radiation field and the external electric field. For pedagogical purpose we discuss the variation of the line shape under the influence of a harmonic field characterized by a variable, but fixed single frequency ω_0 first. We then present the calculation of the actual fluctuating microfield by MD simulations. In Section 3 we test the validity of the quasi-static and impact approximations and calculate the shape of the Ly_α–lines in hydrogen and aluminium for a wide range of plasma densities and temperatures from weakly to very strongly coupled plasmas. We compare our calculations in Section 4 with recent experiments performed in Jena [17] and in Garching [18–20]. This leads to the conclusion that the traditional approximations, impact for the electrons and quasi-static for the ions, cease to be valid for the plasma states already reached in the present experiments (see Sect. 5). The intermediate strongly coupled regime will become even more important for the planned free-electron-laser (X)FEL facilities.

2 Radiating hydrogen-like ions in fluctuating electric microfields

In this section we describe the solution of the wave equation for a hydrogen-like ion coupled to the radiation field and to a time-dependent external electric field. As an example we study the transition from the impact to the quasi-state regime for the Ly_α–line in an oscillatory monochromatic field. The actual fluctuations in the plasma are calculated by MD simulations.

2.1 Wave equation for a radiating, hydrogen-like ion in a time-dependent electric field

We first consider a one-electron ion in the radiation field and an external time-dependent electric field. The Hamiltonian is the sum of H_a describing the unperturbed ion. H_γ for the free radiation field, H_i describing the interaction between the electron and the radiation field and a dipole term $e\vec{x}\cdot\vec{E}(t)$ for the interaction between the electron (charge $-e$, distance $\vec{x}$ from nucleus) and the external field $\vec{E}(t)$

$$H = H_\gamma + H_a + H_i + e\vec{x}\cdot\vec{E}(t). \tag{2.1}$$

The individual terms have the following structure:

(i) the radiation field consists of modes $|\lambda\rangle$ with frequencies ω_λ which are created and annihilated by operators b_λ^+ and b_λ, respectively,

$$H_\gamma = \sum_\lambda \hbar\omega_\lambda b_\lambda^+ b_\lambda; \tag{2.2}$$

(ii) the electron with mass m_e moves in the potential of a nucleus with charge Ze. In the present application it turns out that it suffices to start from the non-relativistic Schrödinger equation

$$H_a|k\rangle = \left(\frac{\vec{p}^2}{2m_e} - \frac{Ze^2}{|\vec{x}|}\right)|k\rangle = \hbar\omega_k|k\rangle \tag{2.3}$$

for the electron state $|k\rangle$ with energy $\hbar\omega_k$. Here $\vec{p}$ is the momentum operator and k is a multi-index including radial, angular momentum and spin quantum numbers. The present calculations are done in the configuration space corresponding to the solutions of equation (2.3). In order to discretize the continuum a boundary condition $\langle\vec{x}|k\rangle = 0$ is imposed at a radius $x = R$, which is chosen sufficiently large in order not to influence the final results. The radial wave functions with this boundary condition are still confluent hypergeometric functions, but the radial quantum numbers of bound states are not integers any more [21]. In order to obtain a finite basis the (former) continuum states are cut off at sufficiently large quantum numbers. Alternatively the continuum could be handled by forming wave packets with a width that must be adjusted appropriately [22]. We have also solved the time-dependent equation (2.1) on a grid for the electron wave function $\langle\vec{x}|k\rangle$ [23, 24]. This has not only advantages for the description of the continuum but is also easier to implement interactions between the radiator and the plasma particles beyond the dipole term in equation (2.1). On the other hand spatially extended states require very large simulation boxes. Quite generally in the present context we found the solution on the grid more expensive numerically than working in configuration space and adopted the latter for the subsequent calculations.

At high Z relativistic corrections must be considered and also the spin should be treated as a dynamical variable. It turns out that in the cases considered here it suffices to include the first-order fine-structure shift [25]

$$\Delta E = \begin{cases} -\frac{|E_n|\alpha^2 Z^2}{n}\left(\frac{1}{l+\frac{1}{2}} - \frac{3}{4n}\right) & l > 0 \\ -\frac{|E_n|\alpha^2 Z^2}{n}\left(1 - \frac{3}{4n}\right) & l = 0 \end{cases}. \tag{2.4}$$

Here n is the principal quantum number of the hydrogen-like ion, E_n the corresponding energy, l the orbital angular momentum quantum number and $\alpha \approx 1/137$ the Sommerfeld constant;

(iii) the interaction with the radiation field results from the minimal substitution $\vec{p} \to \vec{P} + e\vec{A}$ in H_a. In dipole approximation the interaction describing the emission of radiation is

$$H_i = \frac{ie}{\hbar}[H_a, \vec{x}] \cdot \sum_\lambda b_\lambda^+ \sqrt{\frac{\hbar}{2\omega_\lambda \varepsilon_0 V}}\ \vec{e}_\lambda. \qquad (2.5)$$

Here ε_0 is the permittivity of the vacuum, V a normalization volume and $\vec{e}_\lambda$ a polarization vector and the absorption of photons from the radiation field has been dropped here from the model, we remind that we wish to study the state of the plasma after the irradiating laser has been switched off.

2.2 The emission of radiation and the power spectrum of the dipole operator

The interaction $e\vec{x} \cdot \vec{E}(t)$ between the radiator and the plasma is time-dependent and possibly strong. Going beyond the second order treatment of reference [14] we use the interaction picture with the unperturbed basis states

$$(H_a + H_\gamma)|k\rangle = \hbar(\omega_k + \omega_\lambda)|k, \lambda\rangle = \hbar\omega_{k,\lambda}|k, \lambda\rangle. \qquad (2.6)$$

The total wave function is

$$|\Psi(t)\rangle = \sum_{k,\lambda} c_{k,\lambda}(t) e^{-i\omega_{k,\lambda}t}|k, \lambda\rangle \qquad (2.7)$$

where the expansion coefficients $c_{k,\lambda}(t)$ describe the nontrivial time dependence according to the system of equations

$$i\hbar\dot{c}_{k,\lambda}(t) = \sum_{k',\lambda'} e^{i(\omega_{k,\lambda} - \omega_{k',\lambda'})t} c_{k',\lambda'}(t) \times \langle k, \lambda|H_i + e\vec{x} \cdot \vec{E}(t)|k', \lambda'\rangle. \qquad (2.8)$$

The transition rate per unit energy interval for the emission of unpolarized photons is then

$$P_Q(\hbar\omega_\lambda) = \frac{e^2\omega_\lambda}{6\pi^2 c^3 \varepsilon_0 \hbar^2} \times \lim_{T\to\infty} \frac{1}{T} \sum_{k'} \left| \int_0^T dt \sum_k e^{i(\omega_{k',\lambda} - \omega_{k,0})t} \times c_{k,0}(t)(\omega_{k'} - \omega_k)\langle k'|\vec{x}|k\rangle \right|^2. \qquad (2.9)$$

The evaluation of P_Q requires the solution of the quantum equations of motion (QEOM), (2.8) in the product space of radiator states and photon modes. Instead we will often use in the applications below a simplified and more economical approach which rests on the power spectrum of the dipole operator. It is defined as the square of the absolute value of the Fourier transform of the expectation value of the dipole operator. Normalizing as above we introduce

$$P_D(\hbar\omega_\lambda) = \frac{e^2\omega_\lambda^3}{3\pi c^3 \varepsilon_0 \hbar^2} \lim_{T\to\infty} \frac{1}{T} \left| \frac{1}{\sqrt{2\pi}} \int_0^T e^{i\omega_\lambda t} \vec{d}(t) dt \right|^2 \qquad (2.10)$$

with the dipole moment

$$\vec{d}(t) = \sum_{k',k} e^{i(\omega_{k'} - \omega_k)t} c_{k'}^*(t) c_k(t) \langle k'|\vec{x}|k\rangle. \qquad (2.11)$$

Here $c_k(t)$ are the expansion coefficients for the solutions $\sum_k c_k(t)|k\rangle$ of the ion in the fluctuating field, i.e. the Hamiltonian $H_a + e\vec{x} \cdot \vec{E}(t)$. In the interaction picture these coefficients are obtained from the system

$$i\hbar\dot{c}_k(t) = \sum_{k'} e^{i(\omega_k - \omega_{k'})t} c_{k'}(t) \langle k|e\vec{x} \cdot \vec{E}(t)|k'\rangle. \qquad (2.12)$$

Let us now consider a transition $k \to k' = g$ downwards to a state $|g\rangle$ which is nearly filled, i.e. $c_{k'} = \delta_{k',g}$. Then the dipole moment in equation (2.11) is calculated with respect to the state $|g\rangle$ and

$$P_D(\hbar\omega_\lambda) = \frac{e^2\omega_\lambda^3}{6\pi^2 c^3 \varepsilon_0 \hbar^2} \lim_{T\to\infty} \frac{1}{T} \left| \int_0^T dt \sum_k e^{i(\omega_g + \omega_\lambda - \omega_k)t} \times c_k(t)\langle g|\vec{x}|k\rangle \right|^2. \qquad (2.13)$$

Under the same assumptions one obtains from the expression (2.9)

$$P_Q(\hbar\omega_\lambda) = \frac{e^2\omega_\lambda}{6\pi^2 c^3 \varepsilon_0 \hbar^2} \lim_{T\to\infty} \frac{1}{T} \left| \int_0^T dt \sum_k e^{i(\omega_g + \omega_\lambda - \omega_k)t} \times c_k(t)(\omega_g - \omega_k)\langle g|\vec{x}|k\rangle \right|^2. \qquad (2.14)$$

For sufficiently weak perturbations the width of the line is small, so that we may replace $\omega_g - \omega_k$ by $-\omega_\lambda$ outside the oscillating factor. So both expressions (2.13) and (2.14) agree.

Of course the total radiated power is underestimated for excited radiators where $|c_g|^2 < 1$. This can be compensated by dividing through the time-averaged occupation probability of the lower state

$$P_D(\hbar\omega_\lambda) \to \frac{P_D(\hbar\omega_\lambda)}{\langle |c_g(t)|^2 \rangle_t}. \qquad (2.15)$$

Most of the subsequent calculations will be done in this dipole power spectrum approximation (DPSA). We will show the validity of this approximation by comparing explicitly P_D and P_Q from the QEOM in Section 3. The DPSA is justified as the emission of radiation through the interaction H_i changes the occupation probabilities of the radiator's states on a much slower scale than the fluctuating fields.

2.3 A radiator in a monochromatic external field

Before embedding the radiating ion in a plasma it seems worthwhile to study the influence of an external field

$$E = E_0 \sin \omega_0 t \tag{2.16}$$

oscillating with a single frequency ω_0 on the structure of the spectral lines of the radiator. Such a model calculation exhibits the transition from the quasi-static regime $\Delta\omega \gg \omega_0$, where the structure of a line is determined by the distribution

$$P(E) = (\pi E_0)^{-1}(1 - (E/E_0)^2)^{-1/2} \tag{2.17}$$

of the electric field (2.16) to the frequency dominated regime $\omega_0 \gg \Delta\omega$. Here

$$\Delta\omega = 3a_Z eE_0/\hbar \tag{2.18}$$

is the Ly_α Stark shift with $a_Z = a_0/Z$ and $a_0 = 4\pi\varepsilon_0\hbar^2/(m_e e^2)$ is the Bohr radius. We show in Figure 1 results for the Ly_α–transition from the occupied $2p$- to the unoccupied $1s$-level. The unperturbed transition energy is $\hbar\omega_{\mathrm{Ly}_\alpha} = (3/8)Z^2e^2/(4\pi\varepsilon_0 a_0) \approx 10.2$ eV for hydrogen. An iterative solution of equation (2.8) starting from the zero-order case $c_{2p}(t) = 1$ corresponding to a line at the Ly_α frequency shows for each iteration step n the appearance of an extra pair of side lines at $\pm n\omega_0$. With decreasing ω_0 more and more strength is distributed among more and more side lines, until the probability distribution (2.17) emerges as an envelope in the quasi-static limit.

2.4 MD simulations of plasma microfields

A one-component plasma (OCP) of particles with charge q is in equilibrium completely described by the coupling (plasma) parameter

$$\Gamma = \frac{q^2}{4\pi\varepsilon_0 a k_\mathrm{B} T}, \tag{2.19}$$

which is the ratio of the pair potential energy and the thermal energy $\beta^{-1} = k_\mathrm{B}T$ of the particles. Here the mean distance a between the particles (Wigner-Seitz radius) is connected to the particle density n by

$$a = (3/(4\pi n))^{\frac{1}{3}}. \tag{2.20}$$

A collective length scale is given by the Debye shielding radius

$$\lambda_\mathrm{D} = (\varepsilon_0 k_\mathrm{B} T/q^2 n)^{\frac{1}{2}} = a(3\Gamma)^{-\frac{1}{2}}. \tag{2.21}$$

With the thermal velocity $v_\mathrm{th} = (k_\mathrm{B}T/m)^{\frac{1}{2}}$ of particles of mass m one obtains the plasma frequency

$$\omega_p = v_\mathrm{th}/\lambda_\mathrm{D} = (q^2 n/(\varepsilon_0 m))^{\frac{1}{2}} \tag{2.22}$$

which sets the collective time scale ω_p^{-1}. The plasma can be described classically if the thermal wave length is smaller than the mean distance a

$$\lambda_\mathrm{th} = (2\pi\hbar^2/(m k_\mathrm{B} T))^{\frac{1}{2}} \ll a. \tag{2.23}$$

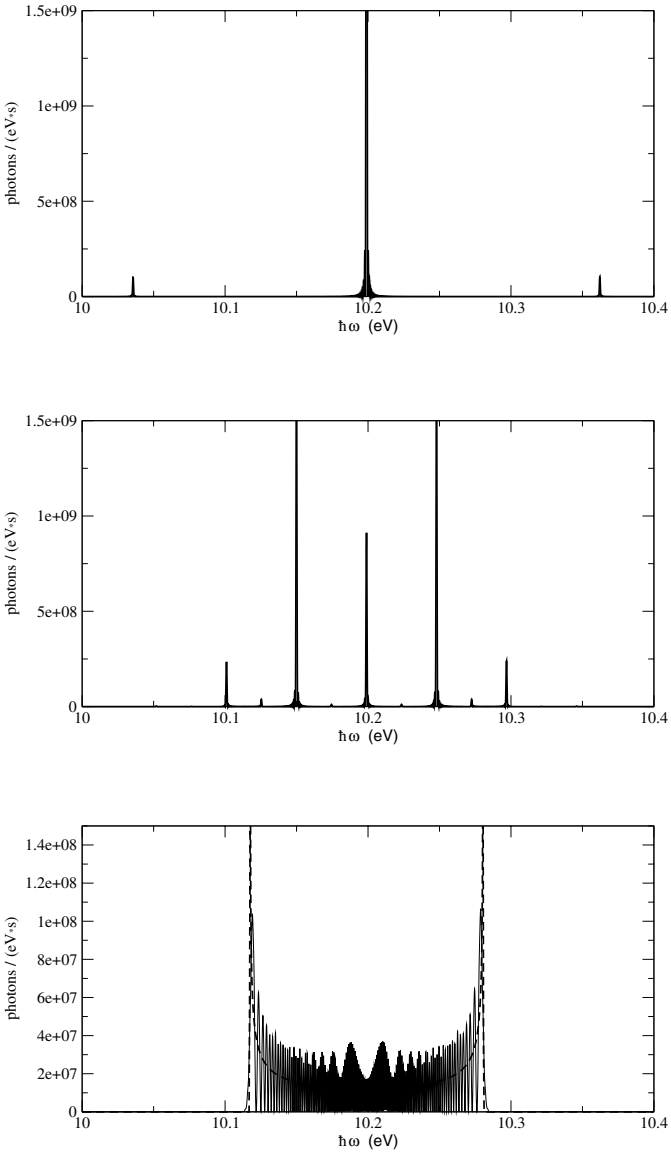

Fig. 1. The emission of the Ly_α radiation in an oscillating field with amplitude $E_0 = 10^{-3}e/(4\pi\varepsilon_0 a_0^2)$ in DPSA (solid curves). The ratio of the Stark shift $\Delta\omega$ to the oscillation frequency ω_0 is 2, 0.3 and 0.005 in the top, center, and bottom panels, respectively. The dashed curve in the bottom panel is the quasi-static distribution (2.17).

Or, equivalently, the degeneracy parameter Θ, i.e. the ratio of the thermal energy and the Fermi energy E_F must fulfill

$$\Theta = k_\mathrm{B}T/E_\mathrm{F} = \frac{2mk_\mathrm{B}T}{\hbar^2(3\pi^2 n)^{2/3}} = 4\pi\left(\frac{4}{9\pi}\right)^{2/5}\left(\frac{a}{\lambda_\mathrm{th}}\right)^2 \gg 1. \tag{2.24}$$

For a nonrelativistic treatment the thermal energy of the particles must be smaller than their rest energy

$$k_\mathrm{B}T/(mc^2) \ll 1. \tag{2.25}$$

We consider hydrogen-like ions as radiators in a completely ionized plasma. Due to their large mass ratio the

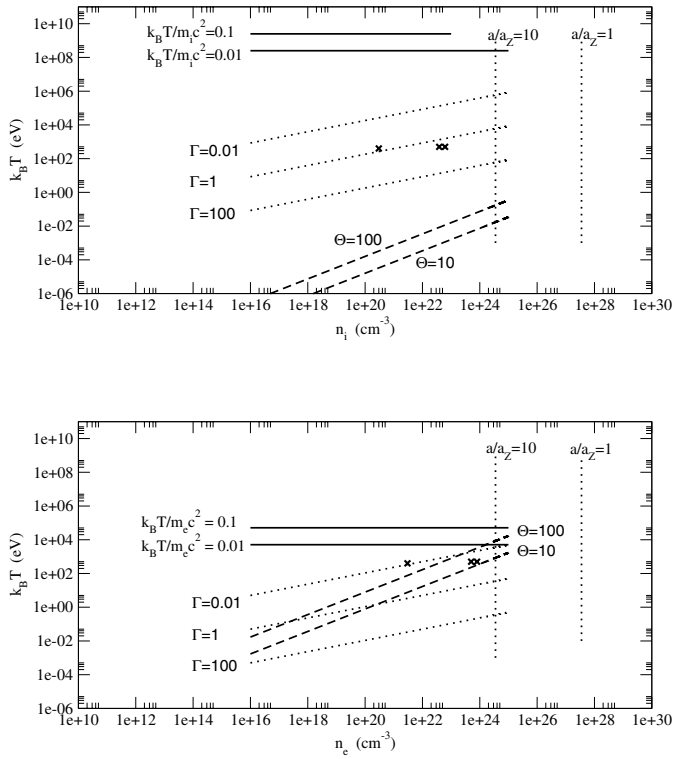

Fig. 2. Areas of validity of the classical nonrelativistic description and working points of the experiments [17,20] (crosses) in the density-temperature ($n - k_{\rm B}T$) plane. The horizontal solid lines show limits for the nonrelativistic description, the vertical dotted lines limits for the dipole approximation. The other dotted lines limit areas of coupling parameters Γ (2.19) and degeneracy parameters Θ (2.24). Upper panel: Al^{13+}, lower panel: electrons.

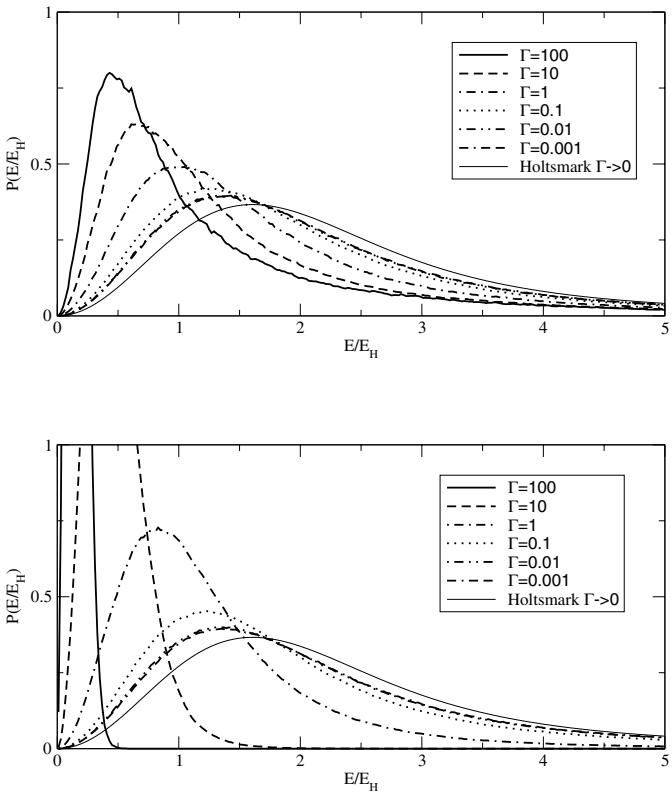

Fig. 3. Distributions for the electric microfield for values of the plasma parameters $\Gamma = 0.001 \ldots 100$ and the Holtsmark distribution. Upper panel for neutral reference points, lower panel for charged reference points.

electrons and the ions move on very different timescales. We will show below that this allows to model the actual plasma as a superposition of two OCP's for the electrons (e) and the ions (i). As we want to compare with experiments on Al-plasmas later, we show in Figure 2 areas of validity for a classical nonrelativistic description of an Al^{13+} OCP in the $n - k_{\rm B}T$ plane. Also shown are vertical lines limiting the validity of the dipole approximation for plasma-radiator interaction used in equation (2.1). For that purpose the mean distance a between the particles must be larger than the atomic length scale a_Z.

As discussed above the distribution of the electric microfield $P(E)$ plays a central role for the line shape. Models for this distribution exist in the limits of an ideal plasma [26], a weakly coupled plasma [27] and for very strongly coupled plasmas [28]. For intermediate cases an effective independent-particle model (APEX) has been developed [11–13]. It rests essentially on the pair distribution function and has been tested by comparison with molecular dynamics (MD) and Monte-Carlo simulations. In order to cover the entire range from small to large plasma parameters we use here classical molecular dynamics (MD) simulations which have been described in detail somewhere else [29]. As an example we show in Figure 3 for an OCP the distributions $P(E/E_{\rm H})$ as function of the electric field scaled in units of the Holtsmark field

$$E_{\rm H} = (8\pi/25)^{\frac{1}{3}} Ze/(4\pi\varepsilon_0 a^2). \qquad (2.26)$$

These distributions were obtained from ensembles of fields taken at charged reference points (i.e. a plasma particle). The coupling parameters range from $\Gamma = 100$ to nearly ideal $\Gamma = 0.001$. It should be noted that the Holtsmark limit $\Gamma \to 0$ can only be reproduced by increasing the size of simulation box beyond any finite limit because of equation (2.21). As the thermal motion of the particles is suppressed with increased coupling the distributions $P(E/E_H)$ and the mean electric fields are shifted towards smaller values.

In principle a plasma consisting of several components should be simulated: the plasma ions, the electrons and the radiators. However, unless the coupling becomes very strong and many bound states are formed, the electrons and ions remain poorly correlated in time. This has the consequence that the dynamics of the microfield fluctuations does not depend very much on the spatial correlations between the ions and the electrons. For that purpose we compare power spectra $|E(\omega)|^2$ of the electric field obtained from simulations of a two-component plasma (TCP) [30] with corresponding OCP results. As shown in Figure 4 the power spectra have a small peak near the electronic plasma frequency $\omega_{p,e}$, but they are dominated

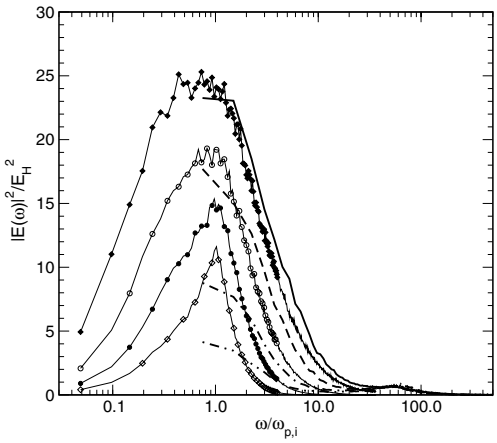

Fig. 4. Normalized power spectra of electric fields at a proton as function of the frequency scaled by the plasma frequency (2.22) of the ions. Solid curve TCP and full diamonds OCP at $\Gamma = 0.5$, dashed curve TCP and open circles OCP at $\Gamma = 1.0$, dashed-dotted curve TCP and full circles OCP at $\Gamma = 2.0$, dashed-double-dotted curve TCP and open diamonds OCP at $\Gamma = 4.0$.

by a peak about the ionic (here protonic) plasma frequency $\omega_{p,i}$. In later applications to experiments [17,20] the frequency range $\omega_0 = (2 \div 5)\omega_{p,i}$ on the right flank of the ionic peak will be relevant in which the TCP spectrum is well reproduced by the ion OCP. For reasons of numerical economy we will subsequently consider a superposition of the two OCP's, one for the ions and one for the electrons. The radiator is then considered to be at a charged reference point with respect to the ions, while it is put at a neutral reference point with respect to the faster moving and less correlated electrons. The time-dependent equations describing the coupling of the microfield to the radiator are then solved for an ensemble of typically thirty independent microfields. This yields finally the mean emission as well as the statistical error (mean error of the mean). Whenever graphically possible we have shown this error as bars in our figures.

2.5 Master equation for the coupling between radiator and plasma

At this stage we have neglected the feedback of the radiator's excitation to the plasma. In this respect the plasma particles move as if they had an infinite mass. As they have a finite velocity it appears as if the radiating electron is embedded in a plasma of infinite temperature. Accordingly the time evolution of the total system will lead to an equal population of all electronic states. As the time-dependent feedback could be implemented only at a very great expense in the MD simulations we enforce a canonical equilibrium state of the plasma and the radiating electron by modifying the interaction in equation (2.12) according to

$$e\vec{x} \cdot \vec{E}(t) \to e^{-\beta H_a/2} e\vec{x} \cdot \vec{E}(t) e^{\beta H_a/2}. \tag{2.27}$$

and similarly in (2.8).

3 Quasi-static and impact approximations

Our description of the emission of radiation as developed in the previous section rests on the solution of time-dependent equations of motion (2.8, QEOM) or (2.12, DPSA) with fluctuating microfields $\vec{E}(t)$ obtained from MD simulations. In the conventional approach one uses the quasi-static and the impact approximations to account for the perturbation of the radiator by the plasma ions and electrons, respectively. In this section we compare these approximations in their range of validity with our simulations. Unless otherwise stated we use here and in the following a basis of $N \approx 50$ atomic states $|k\rangle$ with orbital angular momenta $0 \le l \le l_{\max} = 2$ and the boundary condition $\langle \vec{x}|k\rangle = 0$ for $x = R = 30a_Z$. The simulations of the plasma are performed with 300 particles of either species, e or i.

The characteristic perturbing frequency is related to the free time of flight of the plasma particles

$$\omega_0 = 2\pi \frac{v_{\rm th}}{a} \propto n^{\frac{1}{3}} T^{\frac{1}{2}} \tag{3.1}$$

as long as the plasma is moderately coupled. In a strongly coupled plasma ($\Gamma \gg 1$) the collective plasma mode with frequency $\omega_p \propto n^{\frac{1}{2}}$ becomes important and sets the scale for the perturbation.

3.1 Quasi-static approximation (QSA)

The typical Stark splitting of the Ly_α–line is

$$\Delta\omega = \frac{3a_Z e\langle E\rangle}{\hbar} \tag{3.2}$$

where

$$\langle E\rangle = \int_0^\infty EP(E)dE \tag{3.3}$$

is the average value of the microfield. In the linear Stark effect two of the four $n = 2$ levels remain unaffected while the electric field shifts two levels by $\pm\Delta\omega$. One expects therefore a strong central peak and wings which reflect the distribution $P(E)$. The asymmetry of the line shape is due to terms beyond the linear Stark effect. With increased coupling the mean microfield $\langle E\rangle$, see Figure 3, and the Stark splitting (3.2) decrease. This is clearly visible in the results shown in Figures 5 and 6 for the Ly_α–line of Al^{12+} in an Al^{13+} plasma at solid state density ρ_0 and temperatures $k_{\rm B}T = 10^3$ eV and 10^5 eV, respectively. We note that the simpler simulation scheme DPSA (2.12) agrees quite well with more involved QEOM (2.8) except for a possible underground, see Figure 6. We will therefore employ the DPSA in the following, while checking and correcting for an underground with a few QEOM calculations in the wings of the line. The quasi-static approximation (QSA) agrees, as expected, with the simulations as soon as the actual distance from the center of the line becomes larger than the perturbing frequency. With decreasing temperature the range of validity increases from the outer wings of

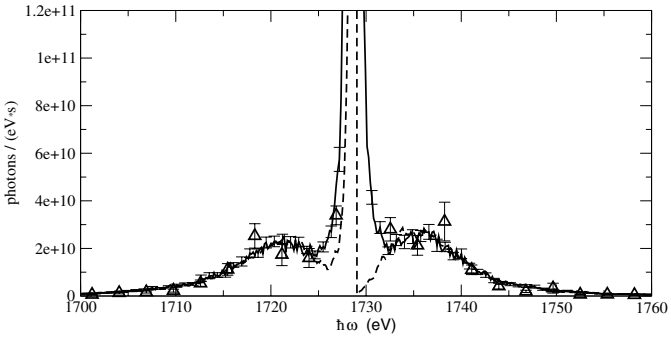

Fig. 5. The Ly$_\alpha$–line in an Al^{13+} plasma at $n_e = 8\times10^{23}$ cm^{-3} (solid state density) and $k_BT = 10^3$ eV. The plasma parameter is $\Gamma = 1.5$, the average value (3.3) of the microfield $\langle E\rangle = 1.1E_H$, and the ratio of the characteristic perturbing time (3.2) to the free time of flight (3.1) is $\omega_0/\Delta\omega = 0.15$. The solid curve is the DPSA, the triangles are the QEOM and the dashed curve is the QSA.

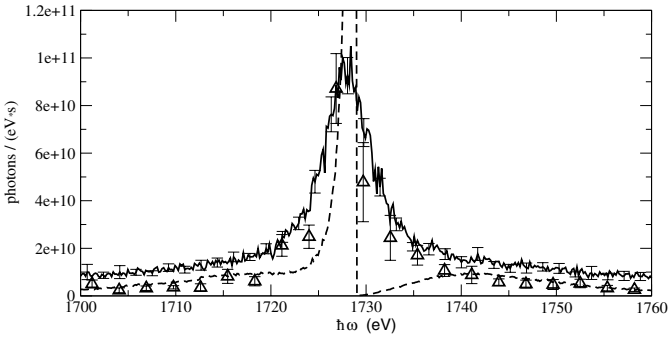

Fig. 6. The same as in Figure 5 for $k_BT = 10^5$ eV, $\Gamma = 0.015$, $\langle E\rangle = 2.5E_H$ and $\omega_0/\Delta\omega = 0.68$.

the line inwards. The ratio of the characteristic perturbing frequency ω_0 (3.1) to the Stark splitting $\Delta\omega$ (3.2) which should be small for the validity of the QSA, $\omega_0/\Delta\omega \ll 1$, decreases indeed from the value 0.68 in Figure 6 to a value 0.15 in Figure 5. Quite generally the shape of the lines becomes broader with increasing temperature and the width of the central peak is underestimated by the QSA.

3.2 Impact approximation (IA)

Although the main emphasis of this paper is on slow, correlated ions we use the opportunity to test some features of the impact approximation for swift electrons. Here the line broadening is due to a statistical perturbation of the line energy [31]. The perturbing particles moving on rectilinear trajectories exert instantaneous statistically independent kicks on the radiator. This smears the energies of both the upper and the lower level. There results a shifted Lorentzian line shape with a width $\omega \propto nT^{-\frac{1}{2}}$. The impact approximation involves thus three assumptions:

(i) a radiator subspace consisting of the $n = 1, 2$ levels for the Ly$_\alpha$ transition;
(ii) the plasma is ideal, i.e. the plasma particles do not interact with each other, but only with the radiator;

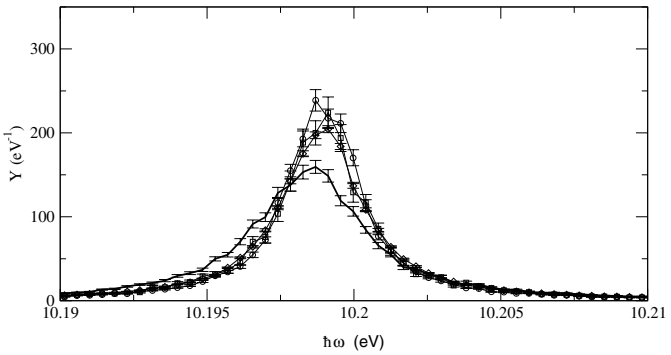

Fig. 7. Normalized spectra of the Ly$_\alpha$–line of an H atom in an electron plasma at $n_e = 2\times10^{18}$ cm^{-3}, $k_BT = 30$ eV, $\Gamma = 10^{-2}$, $\langle E\rangle = 2.6E_H$, $\omega_0/\Delta\omega = 79$. The solid curve is the DPSA, the circles are the DPSA′, the squares are the IA′ and the diamonds are the IA.

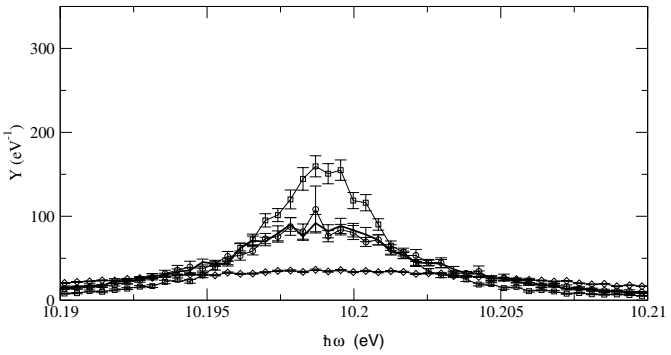

Fig. 8. As Figure 7 for $k_BT = 0.1$ eV, $\Gamma = 3$, $\langle E\rangle = 2.0E_H$, $\omega_0/\Delta\omega = 5.9$ and $\omega_p/\Delta\omega = 2.8$.

(iii) the collisions with the radiator are instantaneous and statistically independent.

In order to test the IA we will in the following use the DPSA as described in Section 3 and implement the assumptions (i), (ii) and (iii) step by step. We will call the restriction (i) to $n = 1, 2$ subspace the restricted dipole power spectrum approximation (DPSA′). If, in addition, the perturbing plasma is treated as ideal but the collisions with radiator remain resolved in time, as in (ii), we label the results by IA′. Finally, if the collisions of the plasma particles with the radiator are instantaneous, with a potential

$$V(t) = -\hbar K\vec{e}\cdot\vec{x}\delta(t - t_0) \tag{3.4}$$

for random kicks of strength K in direction $\vec{e}$ we have also implemented assumption (i) and thus the IA. The kicks (3.4) lead to jumps in the radiator wave function in the subspace

$$\Psi(t_0^+) = \exp K\vec{e}\cdot\vec{x}|\Psi(t_0^-)\rangle. \tag{3.5}$$

For an explicit example we consider in Figures 7 and 8 a H-atom (neutral reference point) in an electron plasma which ranges from nearly ideal to moderately correlated. In the case of the nearly ideal plasma at high temperature, $\Gamma = 10^{-2}, T = 30$ eV and $\omega_0/\Delta\omega = 79$ shown in Figure 7 the approximations DPSA′, IA′ and IA agree

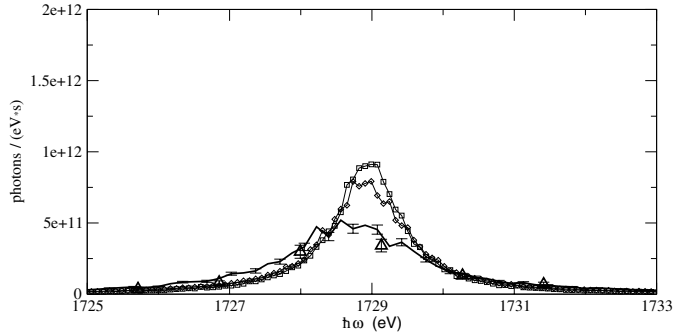

Fig. 9. The Ly_α–line of an Al^{12+} in an electron plasma at $n_e = 8 \times 10^{23}$ cm^{-3} (solid state density) and $k_\mathrm{B}T = 10^3$ eV, $\Gamma = 0.022$, $\langle E\rangle = 2.5E_\mathrm{H}$, $\omega_0/\Delta\omega = 83$. The triangles are the QEOM, the solid curve is the DPSA. The squares and the diamonds are the IA′ and the IA, respectively, both normalized to the DPSA.

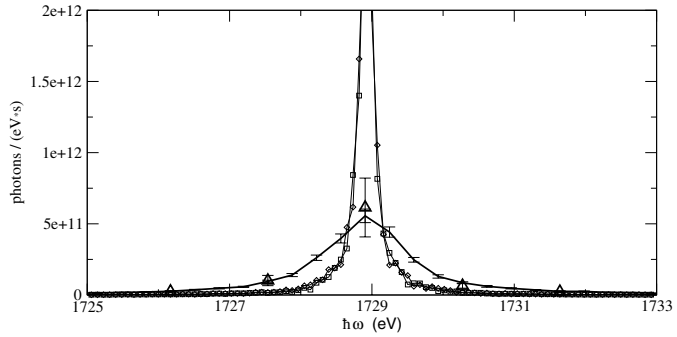

Fig. 10. As Figure 9 for $k_\mathrm{B}T = 10^5$ eV, $\Gamma = 2.2 \times 10^{-4}$, $\langle E\rangle = 2.6E_\mathrm{H}$ and $\omega_0/\Delta\omega = 800$.

among each other. But the comparison to the broader and slightly red-shifted peak obtained in the DPSA shows that the restriction to the $n = 1, 2$ subspace is not valid here. If the temperature is lower, $T = 0.1$ eV, $\Gamma = 3, \omega_0/\Delta\omega = 5.9$ (Fig. 8) on the other hand, it suffices to neglect higher excited states, but the collisions with the radiator must be resolved in time and correlations begin to matter: while the DPSA and DPSA′ agree the simulations with an ideal plasma give a peak that is too sharp or too broad in the IA′ and in the IA, respectively.

We will later compare with experiments on Al and show therefore in Figures 9 and 10 some results for the Ly_α–line of Al^{12+} in an electron plasma at solid state density ρ_0 for $T = 10^3$ eV ($\Gamma = 0.022$, $\omega_0/\Delta\omega = 83$) and $T = 10^5$ eV ($\Gamma = 2.2 \times 10^{-4}$, $\omega_0/\Delta\omega = 800$). The QEOM agrees well with DPSA, but as in Figure 7 the restriction to the $n = 1, 2$ subspace inherent in the impulse approximation IA and in IA′ yields a line shape which is too sharp. Quite generally the width of the line decreases with increasing temperature.

3.3 Al spectra in the n−T plane

In this subsection we will put together the results obtained so far and calculate the shape of the Ly_α line of Al^{12+} in a wide array of plasma parameters see Figure 2. For that purpose we start from the line as it is broadened by the Al^{13+} ions in the plasma. The contribution of the ions to the total width of the line is given in Table 1. It should be noted, however, that the FWHM is not sufficient to characterize the ionic contributions to the line shape, see Figures 5 and 6. Then we fold with the weighted fine structure shift (2.4) which is $\Delta E = 1.29$ eV and account for the Doppler effect [31] which broadens a line with unperturbed frequency $\overline{\omega}$ according to a Gaussian distribution

$$L(\Delta\omega) = \frac{1}{\sqrt{2\pi}\sigma} \exp\left(-\frac{1}{2}\left(\frac{\Delta\omega}{\sigma}\right)^2\right) \tag{3.6}$$

where $\Delta\omega = \omega - \overline{\omega}$ and

$$\sigma^2 = \frac{k_\mathrm{B}T\overline{\omega}^2}{mc^2}. \tag{3.7}$$

Finally we fold to account with the broadening due to the electrons in the plasma, see Table 1.

We discuss now the shape of the Ly_α–line and the contributions of the individual mechanism to the total width for densities $0.1\rho_0$ ($n_e = 8 \times 10^{22}$ cm^{-3}) and $k_\mathrm{B}T = 10^{2\ldots5}$ eV, ρ_0 ($n_e = 8 \times 10^{23}$ cm^{-3}) and $k_\mathrm{B}T = 10^{2\ldots5}$ eV, $10\rho_0$ ($n_e = 8{\times}10^{24}$ cm^{-3}) and $k_\mathrm{B}T = 10^{3\ldots5}$ eV. At smaller temperatures the electrons leave the classical regime, see Figure 2. At $\rho = 0.1\rho_0$ and low temperatures the total width is dominated by the fine structure with some additional electronic broadening. At high temperatures the Doppler broadening is most important, see Table 2, followed by the ionic contribution. So at this low density the plasma effects discussed here do not yet influence the shape of the line very much. This is also visible in Figure 11 where calculations with the DPSA on one hand the quasi-static approximation (QSA) for the ions and the impact approximation (IA) for the electrons on the other hand are compared.

The individual contributions to the total width at solid state density ρ_0 are listed in Table 1. With increasing temperatures ionic and Doppler broadening become more and

Table 1. FWHM-contributions (in eV) by the Al^{13+}-ions and the electrons to the total width of the Ly_α–line in Al^{12+}.

		$k_\mathrm{B}T$ (eV)			
n_e (cm^{-3})		10^2	10^3	10^4	10^5
8×10^{22}	ions	0.20	0.36	0.80	1.90
	electrons	0.37	0.23	0.23	0.18
8×10^{23}	ions	0.37	1.10	2.34	5.46
	electrons	2.64	1.91	1.06	1.27
8×10^{24}	ions		4.46	11.04	84.40
	electrons		15.66	11.59	7.70

Table 2. Doppler broadening (FWHM) of the Ly_α–line in an Al plasma.

$k_\mathrm{B}T$ (eV)	10	10^2	10^3	10^4	10^5
FWHM (eV)	0.08	0.26	0.81	2.57	8.12

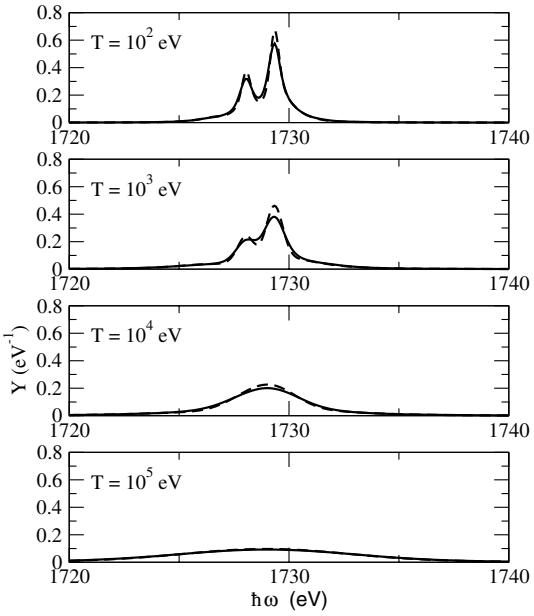

Fig. 11. Normalized spectra of the Ly$_\alpha$–line in an Al-plasma at $n_e = 8 \times 10^{22}$ cm^{-3}. The solid curves are the DPSA, the dashed curves result from the QSA for the ions and the IA for the electrons.

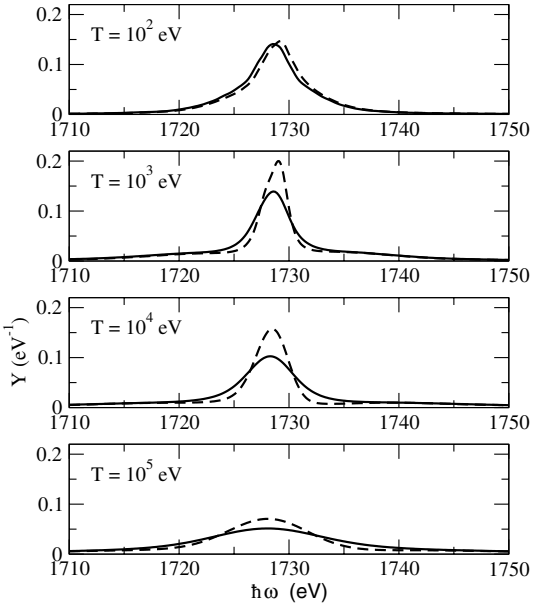

Fig. 12. The same as in Figure 11 for solid state density $n_e = 8 \times 10^{23}$ cm^{-3}.

more important. The quality of the approximations IA for the electrons and QSA for the ions deteriorates with increasing temperature, see Figure 12. The agreement at $T = 10^2$ eV is fortuitous as two errors compensate each other.

These trends are even better observable at $\rho = 10\rho_0$ (Fig. 13), where the plasma effects dominate, in particular at high temperatures the ionic broadening with its characteristic wings. Due to the large density the electric fields become sufficiently strong to cause asymmetric shapes due to nonlinear coupling.

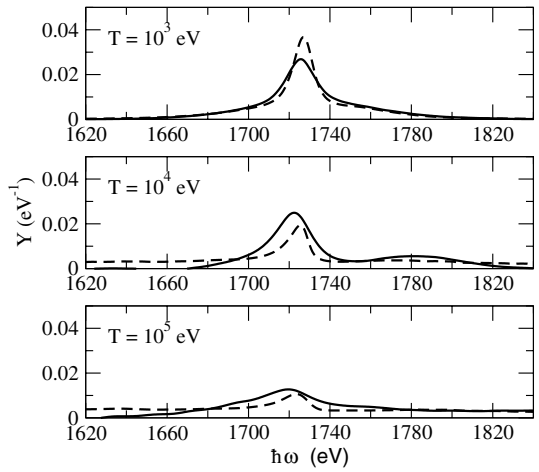

Fig. 13. The same as in Figure 11 for $n_e = 8 \times 10^{24}$ cm^{-3}.

4 Comparison with experiments

The systematic investigations of the previous section show that the standard approximations become doubtful if the plasma density reaches that of the solid state. In the last years experiments have approached this regime. In the following we will compare our calculations with the results of experiments performed in Jena [17] and in Garching [18–20]. We note that the theoretical models discussed so far assume a homogeneous equilibrium plasma. Of course this is not the state in which the laser leaves the target after the irradiating pulse. In particular self-absorption due to plasma inhomogeneities leads to an additional line broadening which is difficult to analyze. Fortunately there has been considerable experimental progress to reduce self-absorption [20].

4.1 The Ly$_\gamma$–line in aluminium at low density

In the analysis of an earlier measurement [17] we will concentrate on the Ly$_\gamma$–line, which is weaker than the Ly$_\alpha$– and Ly$_\beta$–lines and thus less prone to self-absorption. The weighted Stark splitting is four times larger than for the Ly$_\alpha$–line (2.18). Here we took into account 30 states of the radiator with $l \leq 3$ and $n \leq 4$ and the cutoff radius has been chosen $R = 100a_Z$ in order to accommodate the spatially extended $n = 4$ states. The radiators are Al^{12+} ions which are perturbed by electrons and Al^{10+} ions. In this connection we note that the charge of the perturbing ions does not matter very much as $n_i = n_e/Z$ so that the smaller charge state is compensated by a higher ion density [21]. The fine structure and the Doppler broadening are taken into account as described in the previous section. The influence of the electrons is quite small.

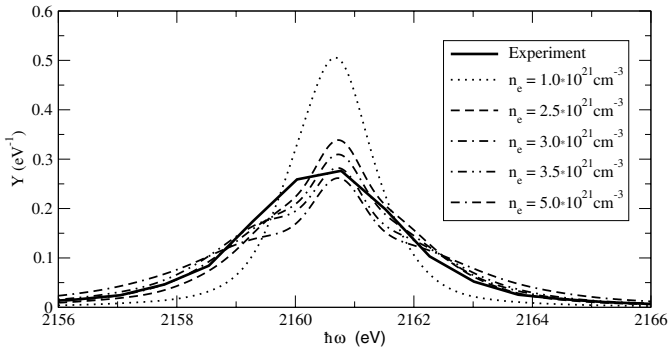

Fig. 14. Normalized spectra of the Ly_γ–line of Al. The solid curve is the measurement after subtraction of the underground and a shift to the theoretical value. The simulated curves (DPSA, $k_\mathrm{B}T = 400$ eV) were folded with the experimental resolution.

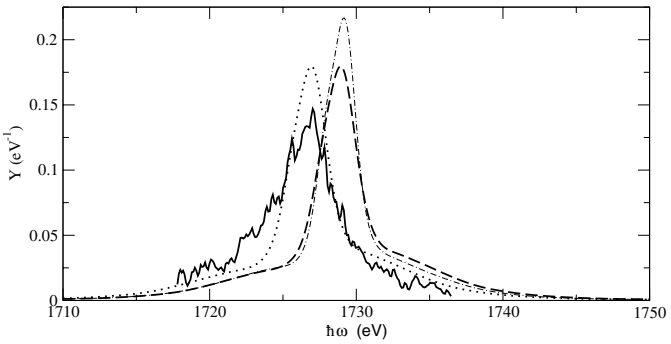

Fig. 15. Normalized spectra of the Ly_α–line in Al. The solid curve is the measurement for a 25 nm layer after subtraction of the underground. The theoretical curves ($k_\mathrm{B}T = 500$ eV, $n_e = 5 \times 10^{23}$ cm^{-3}) include the experimental resolution (0.9 eV), the dashed curve is the DPSA simulation, the dashed-dotted curve is the QSA for the ions and the IA for the electrons. The dotted curve is the DPSA simulation redshifted by 2 eV.

The temperature has been estimated independently from the high frequency part of the total spectrum. We adopt the value $k_\mathrm{B}T = 400$ eV and use our model to determine the density. For that purpose the experimental underground was subtracted, the position of the line, which was only measured relative to other lines, was shifted to the theoretical value and the theoretical profile was folded with the experimental resolution $\hbar\Delta\omega \approx 0.43$ eV. As shown in Figure 14 this allows to fix the density at values near $n_e = 3 \times 10^{21}$ cm^{-3}. The agreement in the wings of the line is excellent, the simulation yields some more structure in the center of the line which is probably masked by self-absorption. An inspection of Figure 2 shows that the criteria for a classical, nonrelativistic treatment of the plasma and the use of the dipole approximation in equation (2.1) are fulfilled. The plasma parameter of the Al^{10+} ions is $\Gamma = 0.43$, the ratio $\omega_0/\omega_{p,i} \approx 6$ justifies the calculation of the microfield in a superposition of OCP's, see Figure 4. It must be kept in mind, however, that this example is not yet a stringent test for our simulations as the line profile is still dominated by the Doppler broadening at this low density.

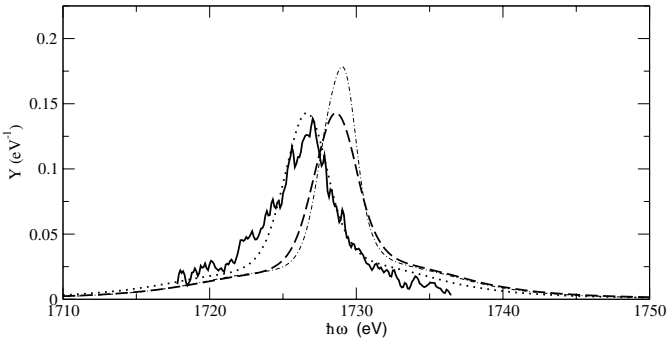

Fig. 16. As in Figure 15 for $n_e = 8 \times 10^{23}$ cm^{-3}.

4.2 The Ly_α–line in Al at solid state density

Earlier experiments on the Ly_α–line in Al^{12+} at solid state density [18,19] were subject to self-absorption in the cooler and less dense surface regions of the target. This can be prevented by using thin (to reduce absorption) target layers with sharp boundaries (to enhance homogeneity). For that purpose a 25 nm Al target layer was embedded in solid carbon at depths ranging from $d = 25$ nm to $d = 400$ nm [20]. With increasing depth the expansion of the Al layer is suppressed and the homogeneity of the Al plasma is improved. In Figures 15 and 16 we compare with an experiment (solid curve) at $d = 400$ nm and $k_\mathrm{B}T = 500$ eV from which the underground has been subtracted. The simulated Ly_α–line (dashed curve) and the line with the approximations QSA for the ions and IA for the electrons (dashed-dotted curve) are folded with the experimental resolution (0.9 eV, FWHM) and compared with the experimental line assuming densities $n_e = 5 \times 10^{23}$ cm^{-3} and 8×10^{23} cm^{-3} in Figures 15 and 16, respectively. The criteria for the classical nonrelativistic treatment of the plasma and the use of the dipole approximation in equation (2.1) are fulfilled, see Figure 2. At $n_e = 8 \times 10^{23}$ cm^{-3} the plasma parameter for the Al^{13+} ions is $\Gamma = 3.16$, the ratio $\omega_0/\omega_{p,i} \approx 2$ justifies the calculation of the microfield in a superposition of OCP's, see Figure 4. The approximations yield narrower shapes than the simulations, which were normalized to the area under the experimental curves. The position of the simulated line must be redshifted by 2 eV. This is the dense plasma line shift (DPLS, Ref. [10], Ch. II 5b) due to the shielding of the electron-nucleus interaction by the plasma particles. Assuming a Debye-shielded interaction instead of the r^{-1}-Coulomb potential first-order perturbation yields a shift of the required magnitude. A comparison of Figures 15 and 16 allows to conclude that the remaining uncertainty in the determination of the density of the target is of order 1×10^{23} cm^{-3}.

5 Conclusions

We have presented a model that works without some assumptions which underly the conventional impact and quasi-static approximations. In particular we

(i) account for the strong correlations among the ions of the plasma;
(ii) resolve the time structure of the microfields;
(iii) account for radiator states including the continuum, which are not directly involved in the transition;
(iv) allow for a nonlinear interaction between the radiator and the plasma to all orders.

We do not only reproduce the impact and quasi-static approximations in the regimes of their validity but our simulations cover a wide area in the density-temperature plane where these approximations become doubtful or even fail. We demonstrate this by a model calculation with a sinusoidal external field as well as for fluctuating microfields obtained from MD simulations of plasmas. We compared our model with recent experiments on Al targets and show that the conventional approximations become marginal under the prevailing conditions.

The quest for more exact treatments beyond the traditional approximations will become even more urgent in connection with experiments at higher densities and temperatures at the planned (X)FEL facilities.

A critical discussion of our results shows that the following improvements are desirable:

(i) the dipole approximation (2.1) for the interaction of the microfield with the radiator suffices for the present experiments [17,20], see Figure 2. In even denser plasmas one must account for close collisions between the radiator and the plasma particles with a quadrupole term in the expansion of the interaction and finally with an exact treatment [14]. In this connection we note that the electron-ion interaction has been studied recently by MD simulations and in theoretical models like the hypernetted-chain-approximation (HNC) [32];
(ii) because of the different time scales we have calculated the fluctuations from the ionic and the electronic component separately, see Figure 4. For even stronger coupled plasmas with many-bound electron-ion states, this becomes questionable. The simulations of the radiator in a two-component plasma is very time-consuming, however;
(iii) relativistic and spin effects beyond the simple fine structure (2.4) can be taken into account by treating the radiator with the Dirac equation [22];
(iv) the major He-like satellite is well separated from the Ly_α–line in the experiment [20]. However, there will be closer satellites due to spectator electrons in higher configurations, which may affect the "red" shoulder of the line. For spectators in the continuum this effect merges into the DPSL. The satellites impose a challenge as they offer an additional tool to determine the temperature of the plasma, see, e.g. chapter 6.3 of reference [31]. For that purpose one has to solve the multi-electron wave equation, for example in the relativistic case the Dirac equation [33].

This work has been supported by the Deutsche Forschungsgemeinschaft (DFG-TO 91/5-3). The authors thank P.-G. Reinhard, I. Uschmann, R. Sauerbrey, G. Soff, W. Scheid and K. Eidmann for many fruitful discussions and G. Zwicknagel and T. Pschiwul for the permission to reproduce unpublished results.

References

1. G.A. Mourou, C.P.J. Barty, M.D. Perry, Phys. Today **51**, 22 (1998)
2. E.M. Campbell, W.J. Hogan, D.H. Crandall, C. R. Acad. Sci. Paris **1**, Série IV, 671 (2000)
3. R. Ramis, S. Atzeni, M. Basko, J. Honrubia, L.F. Ibarez, K.J. Lutz, J. Maruhn, J. Meyer-ter-Vehn, J. Ramirez, J. Sanz, M. Temporal, Nucl. Instr. Meth. A **464**, 45 (2001)
4. P.M. Celliers, G.W. Collins, L.B. DaSilva, D.M. Gold, R. Cauble, R.J. Wallace, M.E. Foord, B.A. Hammel, Phys. Rev. Lett. **84**, 5564 (2000)
5. R. Redmer, Phys. Rep. **282**, 35 (1997)
6. D. Saumon, W.B. Hubbard, G. Chabrier, H.M. van Horn, Astrophys. J. **391**, 827 (1992)
7. D. Habs, G. Pretzler, A. Pukhov, J. Meyer-ter-Vehn, Progr. Part. Nucl. Phys. **46**, 375 (2001)
8. W. Theobald, R. Häßner, R. Kingham, R. Sauerbrey, R. Fehr, D.O. Gericke, M. Schlanges, W.-D. Kraeft, K. Ishihawa, Phys. Rev. E **59**, 3544 (1999)
9. T. Feurer, A. Morak, I. Uschmann, Ch. Ziener, H. Schwoerer, Ch. Reich, P. Gibbon, E. Förster, R. Sauerbrey, K. Ortner, C.R. Becker, Phys. Rev. E **65**, 016412 (2002)
10. R. Griem, *Spectral line broadening in plasmas* (Academic Press, New York, 1974), Ch. II
11. C.A. Iglesias, J.L. Lebowitz, D. MacGowan, Phys. Rev. A **28**, 1667 (1983)
12. J.W. Dufty, D.B. Boercker, C.A. Iglesias, Phys. Rev. A **31**, 1681 (1985)
13. D.B. Boercker, C.A. Iglesias, J.W. Dufty, Phys. Rev. A **36**, 2254 (1987)
14. G.C. Junkel, M.A. Gunderson, C.F. Hooper Jr, Phys. Rev. E **62**, 5584 (2000)
15. D.A. Haynes, D.T. Garber, C.F. Hooper Jr, R.C. Mancini, Y.T. Lee, D.K. Bradley, J.A. Delettrez, R. Epstein, P.A. Janimaagi, Phys. Rev. E **53**, 1042 (1996)
16. S.P. Regan, J.A. Delettrez, R. Epstein, P.A. Janimaagi, B. Yaakobi, V.A. Smolynk, F.J. Marshall, D.D. Mayerhofer, W. Scha, D.A. Haynes Jr, F.E. Golovkin, C.F. Hooper Jr, Phys. Plasmas **9**, 1357 (2002)
17. E. Förster, E.E. Fill, K. Gäbel, H. He, Th. Missalla, O. Renner, I. Uschmann, J. Wark, J. Quant. Spectrosc. Radiat. Transfer **51**, 101 (1994)
18. A. Saemann, K. Eidmann, I.E. Golovkin, R.C. Mancini, E. Andersson, E. Förster, K. Witte, Phys. Rev. Lett. **82**, 4843 (1999)
19. K. Eidmann, A. Saemann, U. Andiel, I.E. Golovkin, R.C. Mancini, E. Andersson, E. Förster, J. Quant. Spectrosc. Radiat Transfer **65**, 173 (2000)

20. U. Andiel, K. Eidmann, P. Hakel, R.C. Mancini, G.C. Junkel-Vives, J. Abdallah, K. Witte, Europhys. Lett. **60**, 861 (2002)
21. J. Marten, thesis, Erlangen (2003)
22. U. Müller-Nehler, G. Soff, Phys. Rep. **246**, 101 (1994)
23. F. Calvayrac, P.-G. Reinhard, E. Suraud, C.A. Ullrich, Phys. Rep. **337**, 493 (2000)
24. E.-M. Reinecke, thesis, Erlangen (2000)
25. H. Friedrich, *Theoretical Atomic Physics* (Springer, Berlin, 1990), Ch. 2.1
26. J. Holtsmark, Ann. Phys. **58**, 577 (1919)
27. C.F. Hooper Jr, Phys. Rev. **165**, 215 (1968)
28. H. Mayer, Los Alamos Scientific Report LA-647 (1947)
29. G. Zwicknagel, C. Toepffer, P.-G. Reinhard, Phys. Rep. **309**, 117 (1999)
30. G. Zwicknagel, T. Pschiwul, private communication
31. D. Salzmann, *Atomic Physics in Hot Plasmas* (Oxford University Press, New York, 1998), Chs. 7.4, 7.5
32. B. Talin, A. Calisti, J. Dufty, Phys. Rev. E **65**, 056406 (2002)
33. K.G. Dyall, I.P. Grant, C.T. Johnson, F.A. Parpia, E.P. Plummer, Comput. Phys. Commun. **55**, 425 (1989)